Liquid Crystals
Publication details, including instructions for authors and subscription information:
http://www.informaworld.com/smpp/title~content=t713926090

Electroconvective dendrites in nematic phases having short range smectic order exhibited by the 4,*n*-alkoxybenzoic acids

B. Katranchev[a]; H. Naradikian[a]; E. Keskinova[a]; M. P. Petrov Corresponding author[a]; J. P. Marcerou[b]
[a] G. Nadjakov Institute of Solid State Physics, 1784, Sofia, Bulgaria [b] Centre de Recherche Paul Pascal CNRS-UPR8641, Avenue A. Schweitzer, 33600, Pessac, France

Online publication date: 12 May 2010

To cite this Article Katranchev, B. , Naradikian, H. , Keskinova, E. , Petrov Corresponding author, M. P. and Marcerou, J. P.(2004) 'Electroconvective dendrites in nematic phases having short range smectic order exhibited by the 4,*n*-alkoxybenzoic acids', Liquid Crystals, 31: 12, 1663 — 1676
To link to this Article: DOI: 10.1080/02678290412331319090
URL: http://dx.doi.org/10.1080/02678290412331319090

Liquid Crystals, Vol. 31, No. 12, December 2004, 1663–1676

Electroconvective dendrites in nematic phases having short range smectic order exhibited by the 4,*n*-alkoxybenzoic acids

B. KATRANCHEV, H. NARADIKIAN, E. KESKINOVA, M. P. PETROV*

G. Nadjakov Institute of Solid State Physics, 72 Tzarigradsko Chaussee Blvd., 1784, Sofia, Bulgaria

and J. P. MARCEROU

Centre de Recherche Paul Pascal CNRS-UPR8641, Avenue A. Schweitzer, 33600, Pessac, France

(*Received 31 July 2003; in final form 19 August 2004; accepted 26 August 2004*)

Electroconvective (EC) dendrites (parabolic type) in nematic (N) liquid crystals with short range smectic order shown by 4,*n*-octyloxybenzoic acid (8-OBA) were observed. The driving of the dendrites by lateral d.c. and a.c. electric field parameters in the nematic temperature range was carried out. The dynamics of dendrite growth were studied and analysed by the Ivantsov two-dimensional solution for the diffusion equation. Using various combinations of blocked and unblocked electrodes, we studied dependences between the dimensionless electric field parameter and product of the dendrite parabolic radius and the velocity of the dendrite growth and found that the type of electrode significantly modifies these basic dependences. We attribute this effect possibly to the opposing ion propagation, i.e. gradient of electric field in direction opposite to that of the charge injection. A possible mechanism of EC dendrite growth is suggested. A comparison with thermal dendrites in liquid crystals is presented.

1. Introduction

Dendrites are the basic microstructural form for most crystalline materials. Usually their growth is controlled by the dimensionless parameter ('distance' from the equilibrium) and in the sense such dendrites have been studied both experimentally and theoretically [1–6]. Dendritic growth is of fundamental interest since the mechanism that leads to the selection of this particular pattern in different systems is very important. Both surface tension and anisotropy produce stable dendrite tips, with sharply defined radii of curvature growing in specific directions [4]. The important role played by anisotropy has been shown for liquid crystal systems [7]. Thermal dendrites of smectic B (SmB)–nematic (N) liquid crystal interface have been observed in [8].

Fluid flow during dendrite growth significantly alters the dendrite structure [1] since the presence of the flow allows the possibility of instabilities due to the flow itself, in addition to the morphological instabilities normally found in crystal growth. The effect of fluid flow on dendrite growth, however, does not exist in thermal dendrites, but always plays an important role in electroconvective (EC) dendrites. Electroconvection in nematic liquid crystals characterised by strong intrinsic anisotropy is a field of intensive study of pattern formation outside of equilibrium [9–11]. The convection of a nematic liquid crystal layer under either an electric field or a thermal gradient offers simple examples of stationary states [12]. An N convective state has been found, which bifurcates continuously from the rest state and is at threshold simultaneously time-dependent and well localized in space, i.e. transition from a stationary to a time-dependent state [13].

Recently Gleeson *et al.* [14–16] indicated EC dendritic growth in the nematic liquid crystal MBBA in the presence of a strong magnetic field, and suggested a complex pattern of convective rolls, which invades the quiescent state in the form of dendrites. These dendrites, similar to the classical example of solidification, grow with constant speed and have an unchanging parabolic shape in the frame of reference moving at that speed. Inside the dendrite structure there is convective flow. The interplay between periodic pattern formation and homogeneous modes is reflected in the phenomenon of EC dendritic growth.

Thermal and EC dendrites show common features. They are accompanied by interface (front) propagation. Such interface propagation could serve as a powerful

*Author for correspondence; e-mail: mpetrov@issp.bas.bg

Liquid Crystals ISSN 0267-8292 print/ISSN 1366-5855 online © 2004 Taylor & Francis Ltd
http://www.tandf.co.uk/journals
DOI: 10.1080/02678290412331319090

tool to distinguish between continuous or second order and weakly first order phase transitions [17]. Time dependence in the pattern evolution has also been considered for binary mixtures [18]. It is therefore relevant to consider the possibility for the system to develop simple time-dependent states.

To date there have been no experiments concerning EC dendrite growth in liquid crystal systems such as 4,*n*-alkoxybenzoic acids (*n*-OBA, where $n=$homologue number) displaying nematic and smectic C phases. Such pattern growth is also interesting since *n*-OBA displays a mesomorphic behaviour due only to the presence of a sufficiently high concentration of dimers, provided via hydrogen bonds. In a set of experiments [19–21] different properties of the N phase of *n*-OBA with $n=7,8,9$ (heptyl, octyl, nonyl) at high and low temperatures were detected. These experiments indicated that due to the temperature variation of the dimer–monomer concentration in the N phase of 7,8,9-OBA, a temperature exists (usually indicated as T^*) that divides the N temperature range into a high temperature N_1 phase (with macroscopic properties of the conventional nematic, e.g. MBBA, PAA) and a low temperature N_2 phase (with smectic – like character). At T^* a strong texture transition is seen, an anomaly of the parameters characterizing the electroconvective instabilities [22], and a dramatic increase of depolarized Rayleigh light scattering [19]; for details see [19–22].

The EC dendrite-like texture observed by us in the N phase of 8-OBA reminds of that observed in [14–16], controlled by a dimensionless parameter (combination of applied electric and threshold field values), and possesses the features of a weak first order phase transition, namely interface (front) propagation and hysteresis. An invasion of the convective state into the equilibrium state is the basic feature of these EC dendrites, thus determining this phenomenon as a first order phase transition, but in a thermodynamically monophase system. This new effect prompts a qualitative and quantitative study of the EC dendrite growth mechanism. The search for common features of thermal and EC dendrites in the same substance is also interesting and is the purpose of the present work.

2. Experimental

2.1. *Materials and sample preparation*

The phase transition temperatures of 8-OBA are:

$$\mathrm{Cr} \overset{101^{\circ}\mathrm{C}}{\longleftrightarrow} \mathrm{SmC} \overset{108{,}1^{\circ}\mathrm{C}}{\longleftrightarrow} \mathrm{N} \overset{146^{\circ}\mathrm{C}}{\longleftrightarrow} \mathrm{I}$$

As previously indicated, direct observation of a full liquid crystal convective structure may be done in a Hele–Shaw (side-view) cell [23, 24]. Electroconvection driven by an a.c. electric field **E** is commonly observed in nematics of positive conductive ($\sigma_a>0$) and negative dielectric anisotropy ($\varepsilon_a<0$) (e.g. MBBA) [9, 25]. In well studied planar aligned cells, where the nematic director **n** is oriented parallel and **E** is applied across the glass plate substrates, this is a phenomenon where experiment and theory match very well. Such liquid crystal cells (LCCs) are considered as standard (top-view) cells, where one can observe the EC patterns in the XY plane for $h \gg d$; here d is the cell thickness and the gap between two electrodes (ITO deposited on the glass plates) and h is the dimension of the liquid crystal film in the X direction. $OXYZ$ is a laboratory coordinate system, where XY is the plane of the glass plates, and OZ is the plate normal. We have used such a standard (top-view) cell to study the electrooptical behaviour in 7,8,9-OBA; the plane of the LCC glass plates is the XY plane, the direction of **n** is the X direction (planar orientation) and **E** is applied across the LCC, i.e. in the Z direction (providing a homogeneous LC geometry $\mathbf{E}\perp\mathbf{n}$) [22]. We compared the results with the well studied case of conventional nematics (e.g. MBBA) where there are no smectic order fluctuations.

In the present experiment we used the side-view (lateral) cell, where $d \approx h$. Here d is the gap between the two lateral electrodes (two silver wires 50–500 μm apart in the Z direction) and h is the LC film dimension in the Y direction (determined by the wire thickness of 50–300 μm). The electric field is again $\mathbf{E}\|Z$, but its direction (Z) is in the XZ plane of the glass plates; Y is perpendicular to this plane and **n** is oriented in the X direction. With this geometry, again ($\mathbf{n}\perp\mathbf{E}$), but we expect to observe a full EC structure indicated by a propagating front in the Z direction between quiescent and convective states in the XZ plane. Thus OX is the direction of **n** orientation imposed by the flow alignment effect. In our case $d \approx h$ and the aspect ratio of the extension of the active area in X to the separation between electrodes d is of the order 10^2. The main difference between this and the standard case is that an indication of EC flow (by small particles) could be observed in the plane parallel to that of the glass substrates.

For a.c. driven EC in liquid crystals it is well known that a rich variety of patterns can be observed [9, 25–29]. The primary EC pattern, the Williams domains, appears as rolls with orientation normal to **n** (NR) for top-view ($\mathbf{E}\perp\mathbf{n}$) geometry; this readily transforms into various secondary instabilities such as the zig-zag instability and the abnormal roll instability, all having very different structures from the dendrite-like structure.

In addition to the type of the cell, in importance, are the sign and the magnitude of $\varepsilon_a=\varepsilon_{\|}-\varepsilon_{\perp}$ and σ_a

($\sigma_{\|}-\sigma_{\perp}$), where the subscripts $\|$ and $\perp$ represent the situations parallel and perpendicular to **n** (optic axis). It has previously been shown [22, 29, 30] that: (i) At large $\varepsilon_a<0$ ($\varepsilon_a<\varepsilon_{ao}=-\delta\sigma_a\varepsilon_{\perp}/(1-\delta\sigma_{\perp})<0$, where $\delta=2(\gamma_1-\gamma_2)/(\gamma_1+2\alpha_4+\beta-2\gamma_2)$ is a Leslie viscosity coefficients combination and $\mathbf{n}\perp\mathbf{E}$ (the direction of **E** is perpendicular to the plane of the glass plate, **n** coincides with the 'rubbing' direction), and the nematic is stable at all electric fields and frequencies. (ii) EC is observed in the NR-conducting regime, at high fields with dynamic scattering (DS) and in 'chevron' domains (dielectric regime) at $\varepsilon_{ao}<\varepsilon_a<0$, $\mathbf{n}\perp\mathbf{E}$. (iii) EC is seen as NR at $0<\varepsilon_a<\varepsilon_{a1}=\varepsilon_{\|}\sigma_a/\sigma_{\|}$. NR is first observed when the field is increased at $0<\varepsilon_a<\varepsilon_{a1}/3$, and then followed by DS: at $\varepsilon_{a1}/3<\varepsilon_a<\varepsilon_{a1}$ only NR are observed since before achieving connection, a reorientation of the N takes place. (iv) At $\varepsilon_a>\varepsilon_{a2}=\varepsilon_{\|}\delta$ and $\mathbf{n}\perp\mathbf{E}$, only a dielectric **n** reorientation (Fréedericksz transition) takes place with increasing voltage and no NR appears since the dielectric moment is stabilizing.

The compound 8-OBA (as well as 7,9-OBA) displays a nematic state characterized by smectic C order fluctuation and small positive anisotropy of the dielectric constant ($0<\varepsilon_a<\varepsilon_{a1}/3$) with an average of over ~ 0.018 the N temperature range [31]. Recently, on changing the sign from $\sigma_a>0$ to $\sigma_a<0$, with decrease in temperature, two different EC patterns in the N phase were observed due to smectic A fluctuation [32]. These high and low temperature EC regimes are similar to those previously found for (7–9)-OBA [22]. Smectic fluctuations in nematics could also change the Leslie coefficients α_3 from negative to positive with temperature decrease [32].

We recall that in a top-view standard cell, with a bent initial deformation for $\mathbf{E}\perp\mathbf{n}\equiv\mathbf{x}$, EC instability is caused by the destabilizing torque M_σ, induced by electroconductivity σ_a, prevailing over both the dielectric (M_ε) and elastic (M_{el}) stabilizing torques. Thus in the stationary condition the molecular orientation is fixed, due to torque balance, even though M_σ is acting. From the dependence $M_\sigma=(-\alpha_2\cos^2\varphi+\alpha_3\sin^2\varphi)G$, where $\varphi(\mathbf{n}\wedge\mathbf{X})$ and $G=-\partial v_z/\partial x$ (the shear rate) induced by the **E** and charge coupling flow, it was indicated that the destabilizing torque in such a geometry is $M_\sigma^{|}=-\propto_2|\partial v_z/\partial x|$ [29, 33, 34]. However, close to the orienting walls, due to the gradient of v_x (the component of the liquid flow along *X*), a stabilizing torque acts which is $M_\sigma^{\|}=\alpha_3|\partial v_x/\partial z|$. Since $|\alpha_3|\ll|\alpha_2|$ [34] and the magnitudes of the gradients $\partial v_z/\partial x$ and $\partial v_x/\partial z$ are comparable, then the stabilizing torque $M_\sigma^{\|}$ only enhances the threshold voltage. Regarding the LCC section *ZX*, when liquid flow is indicated (flow velocity **v** has two components $\pm v_z, \pm v_x$) and a distribution of **n** due to the torque balance is achieved, it is found that the gradient $\partial v_x/\partial z$ (or v_x component) is not an orienting action near to the orienting surface, where the *X* orientation is maintained; $\partial v_z/\partial x$ is the gradient driving the EC.

This theoretical result, expressing the known Carr–Helfrich mechanism [9, 25, 29] for a standard planar LCC, has been confirmed experimentally by many authors mainly for $\varepsilon_a<0$ and $\sigma_a>0$. In the case $\mathbf{n}\|\mathbf{E}\|\mathbf{Z}$ (homeotropic orientation), it has been indicated that EC is possible for $\varepsilon_a>0$, $\sigma_a<0$ in a nematic with smectic fluctuations [33]. At homeotropic orientation $M_\sigma^{|}=\alpha_3(\partial v_z/\partial x)$, and contrary to the planar case, this torque is destabilizing since it enhances the starting molecular tilt (α_3 is negative) [29]. EC could also appear for $\varepsilon_a=0$ at large voltages by grid patterning [28]. Thus the appearance and form of EC (primary or secondary instability) depends significantly on this combination of material parameters, LCC geometry and $M_\sigma^{|}$, $M_\sigma^{\|}$ correlation in the torque balance.

The Fréedericksz transition (homogeneous **n** distortion) can compete with the non-equilibrium EC instability of the basic state. This effect is more pronounced in a top-view LCC for nematics with slightly positive ε_a and $\sigma_a>0$, implying anisotropy of material constants such as those of 8-OBA at $T>T^*$ [22, 34]. The EC becomes possible above a frequency-dependent threshold voltage $U_{th}(f)$. The Fréedericksz transition occurs only for an applied voltage of amplitude U above a certain threshold $U_F=\pi(K_{ii}/\varepsilon_a\varepsilon_o)^{1/2}$ (K_{ii} being the bend or splay elastic constant), since opposing torques from the orientational elasticity must be overcome. Consideration of the expressions for U_F and $U_{th}(0)$ reveals that the Fréedericksz transition is easily preempted by a primary EC instability at small f and moderate ε_a [22, 25, 34]. Thus bistability between the convection states and the homogeneous Fréedericksz distortion is possible, since a bifurcation at the lines U_{th}, U_F is supercritical (forward). The bifurcation is however subcritical and hysteretic at a higher voltage value $U_{th}^F(f)>U_F>U_{th}(f)$. So if ε_a and σ_a are slightly positive the LCC system shows interesting nonlinear EC states, which result from competition between a convection mode and a homogeneous bend or splay mode.

We note that up to now prediction of the EC onset took into account correlation of the material constants σ_a, ε_a, α_2, α_3 as well as the role of the stabilizing and destabilizing torques $M_\sigma^{\|}$ $M_\sigma^{|}$, thus capturing the convection phenomena for any set of parameters [9]. Taking into account the peculiarity of the nematics with short range smectic order used here, we shall make an analogy in later discussion.

Two silver wires (50–300 μm thick) were assembled to produce a liquid crystal cell with lateral electrodes.

Either a.c. or d.c. electric fields were used for EC dendrite growth control. In such a side-view LCC, different from the standard (top-view) LCC previously used for the EC study of 8-OBA [22], we can directly observe full convective structures in a way similar to that in [23]. In order to perform the experiment with blocked electrodes, eliminating the contribution of isotropic instabilities by local charge injection, we used a set of electrode covering materials, such as Mylar sheets, lacquer, tissue and polyimide layers.

Problems connected with electrochemical reaction in the LC is not a subject of this study; we can consider only some physical consequences following from processes close to the electrodes. If the LCC is in a d.c. or low frequency electric field, ions pile strongly at the electrodes; although a possible regeneration of the ions, resulting in a non-homogeneous distribution of charge along the electric field direction, is expected. The maximum potential of the field is near to the electrode, where a double electric layer is developed.

The liquid crystal orientation was obtained only by a 'flow alignment' effect, realized via capillary action during the LCC filling in the isotropic state. The LCC prepared in this way provides for homogeneous alignment of the nematic director **n**.

The EC dendritic texture was observed through a polarizing microscope, Carl Zeiss NU 2, equipped with a hot stage and an automatic temperature control, Linkam TMS 90. For an interelectrode distance larger than 500 µm neither electroconvective nor dielectric orientation effects could be obtained. The onset of EC convection was detected by transmitted polarized light intensity analysis, using a video camera and suitable software.

2.2. *Microtexture polarization analysis of EC dendrites in 8-OBA*

An example of a single EC dendrite growing in 8-OBA under a d.c. electric field is shown in figure 1. This EC dendrite is of parabolic type, similar to that previously observed [14–16]. Such a structure emerges at $T > T^*$ after the applied voltage $U = \mathbf{E}.d$ is raised from zero to some value above the critical voltage U_{th} above which the onset of bifurcation from conduction to convection occurs. This onset is visualized as strip-like (black and white) parabolic convective rolls. Because of the horizontal temperature gradient, the parabola is not completely symmetric in this case, but the dendritic structure is rich in black and white stripes. Such dendrite-like texture grows in the Z direction, perpendicular to the 'easy' direction $\mathbf{n}_o \| X$. The geometrical parameters of the parabolic EC dendrite are the radius of curvature ρ, the interface between the

Figure 1. Electroconvective dendrite of 8-OBA in the presence of a d.c. electric field, $U = 65$ V, $d = 350$ µm. Crossed polarizers $\mathbf{P} \perp \mathbf{A}$. The white bar marked perpendicular to the electrode (the black band), a silver wire, its length indicating the picture size. $\mathbf{n}_o$ is the 'easy' direction.

quiescent state and convective state (normally the distance between the centers of the one black and white stripes) m, and the distance l between the centre of the EC dendrite nuclear location O and dendrite tip A; see figure 2. Due to strong smectic order fluctuations, below T^* no regular time-dependant localized EC parabolic rolls can be detected, although a threshold

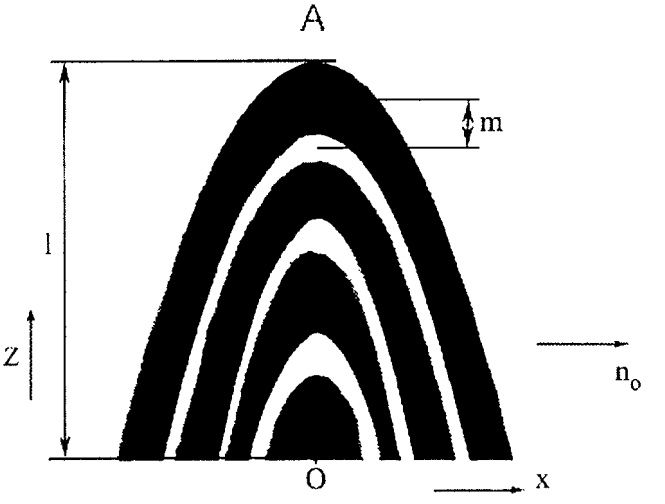

Figure 2. Scheme of an EC dendrite with the geometrical parameters: l = distance of propagation, m = the interface width, O is the centre of nucleation. The centres of the dendrite nucleation start on the positive electrode. *OXYZ* is the laboratory coordinate system.

for EC convection onset can be seen, in a texture consisting of fragmented rolls [19, 20].

In the dynamics of the EC dendrite growth, U_{th} is higher than the known critical field for the Fréedericksz transition. Figure 1 indicates that on a microtextural level, variation in refractive (extraordinary) index caused by the director distortion results in the successive focusing of parallel polarized light, allowing convective flow to be visualized. Note that figure 1 represents the moment of reaching the voltage U_{th} at which the propagation front between convection and quiescent states is still defined. The front moves with velocity $\mathbf{v}$ in the laboratory frame (X,Y,Z) in the Z direction (see figure 2). Above a higher voltage $U_c > U_{th}$ (U_c is the voltage where the propagating front, white or black stripe, between convection and quiescent states is still defined) the system exhibits chaotic behaviour (like the dynamic scattering at a conducting EC instability in a nematic with $\varepsilon_a < 0$ [25]), and no steady-state, parabolic shaped dendrite growth can be obtained. Thus the fundamental dynamic parameter of the EC dendrite growth is $\mathbf{v}$, measured in our case by increase of l with time, $l(t)$. For the measurement of $\mathbf{v}$ we use the Adobe Premiere video technique, by which we are able to resolve the dendrite growth time into small intervals (ms). Normally $\mathbf{v}$, ρ and m are measured simultaneously with variation of U, up or down, thus detecting the response and decay (relaxation) processes of the EC dendrite evolution.

At low d.c. voltages, dendrites always start from the positive electrode or from small inhomogeneities; at larger voltages, they grow very rapidly in many places simultaneously. As we are interested in examining a single dendrite, this implies a particular upper limit on the value of U. The dendrites always originate in pairs (at the other electrode similar dendrites are generated with a higher threshold), which then travel in opposite directions at the same velocity. As mentioned above, the dendrite interface has a non-zero width m; the dendrites are not sharp and differ also from thermal dendrites observed for the same substance *n*-OBA [35]. Nevertheless, along any given radial direction, there is a darkest point of minimum intensity. In making measurements at different values of the applied electric field between U_{th} and U_c we are limited by two factors: one, as already mentioned, concerns the range of U for which steady state dendrite growth is possible; the other is the precision with which we can observe the tip radius of curvature, the velocity of the tip and the interface width. While varying the control parameters, large number of images are recorded and then analysed.

Using the same side-view LCC geometry and in order to explore the role of the slightly $\varepsilon_a > 0$ and smectic order fluctuation in 8-OBA, we have obtained a picture of a conventional N (PAA) with $\varepsilon_a < 0$. This picture is similar to that observed in [23] for MBBA, but different from figure 1 in relation to the set of black and white rolls typical of the dendrite texture. The top-view patterns, for comparison with patterns of the side-view case considered here, above and below T^* for 8-OBA, are indicated in figures 3 (*a*) (strip-like) and 3 (*b*) (cell-like EC texture), respectively. The patterns formed in this geometry are not localized in space, so no dendrite-like texture was observed, see [22].

3. Electric field and temperature driving of the EC dendrites: quantitative analysis

3.1. *Electric field frequency driving of the EC dendrites*

As indicated above, from the variation of the sign and magnitude of the material characteristics ε_a, σ_a, in combination with the experimental top-view standard geometry ($\mathbf{n} \| \mathbf{E}$, $\mathbf{n} \perp \mathbf{E}$), a set of primary and secondary

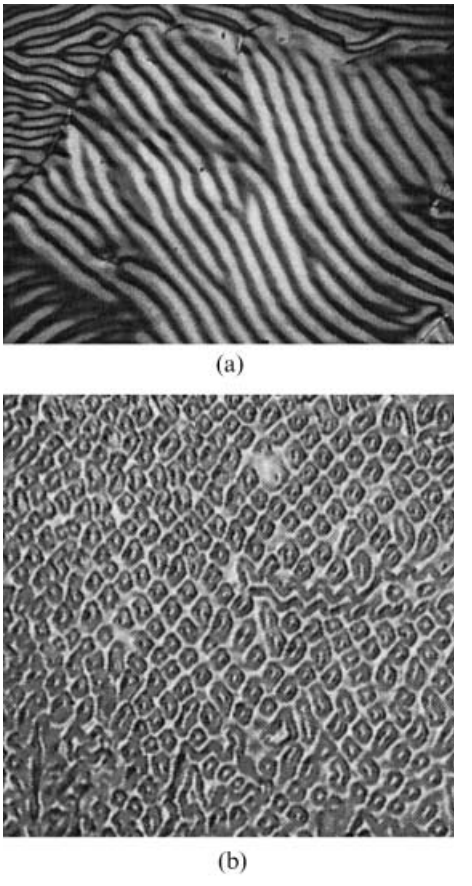

Figure 3. EC in 8-OBA in top-view geometry: (*a*) strip-like EC texture at $U_{th} = 15$ V(d.c.), $T = 138^\circ C > T^*$; (*b*) cell-like EC texture at $U_{th} = 20$ V(d.c.), $T = 110^\circ C < T^*$. The LCC thickness is 20 μm; crossed polarizers; magnification 250×, the same as that of figure 1.

domain textures, provided by the Carr–Helfich mechanism, can be obtained [9, 25, 29]. The nonlinearity of the EC instability and the threshold character of the domain picture appearing in addition to the Fréedericks transition, could be considered as a phase transition in a single thermodynamic system. In such a system, however, one cannot observe the basic characteristic of a first order phase transition—interface (front) propagation of the 'metastable' (disordered) into the stable (ordered) state and corresponding hysteresis [17]. The outline of the EC dendrites (see figure 1) indicates that these EC textures, display front propagation. Both the front propagation and hysteresis give the possibility that the transition from the quiescent (non-convective) state may be related to the criterion of a first order phase transition. On the other hand the evolution of EC parabolic-type rolls in a lateral electric field, and the underlying anisotropy of the LC state, suggest that the Ivantsov solution [36, 37] may be applied to the boundary value problem, for the diffusion equation to be used. We are therefore interested by the relationship between the velocity of a dendrite tip (**v**), the shape of the tip (expressed by ρ and m) and very important driving dimensionless parameter $\Delta=(U^2-U_{th}^2)/(U_c^2-U_{th}^2)$, introduced by analogy with dimensionless supercooling at the thermal dendrites [35, 37, 38].

A peculiarity is seen in electroconvection in a nematic which precedes (on cooling) a SmC phase (e.g. 8-OBA), and which is characterized by short range smectic order [22]. The most typical feature of this EC (at $\varepsilon_a=0.018$) is that, due to strong smectic order fluctuations leading to large smectic-like supramolecular complexes below T^* and a corresponding change of the sign of σ_a (from $\sigma_a>0$ to $\sigma_a<0$, meaning that σ in the layer is larger than in the **n** direction), at this temperature (T^*) a strong anomaly in the EC threshold is observed. Also, due to the very small positive ε_a and the strong smectic C order fluctuation, an interesting competition between the EC instability domain threshold and the Fréedericksz transition is observed for top-view geometry (**n**$\perp$**E**) [22].

Using the classical dependence $U_{th}^2(f^2)$ for 8-OBA [25], we found the relationship between the EC domain threshold U_{th} at $f\to 0$, $U_{th}(0)$, and the Fréedericksz threshold U_F. From this dependence, as well as by the trends of $U_{th}(0)^2$ and $U_F^2=f(T)$, it can be seen that the EC threshold may be lower, close to or higher than U_F, indicating the competition between EC and Fréedericksz transitions, similar to that found previously [34]. When $U_{th}>U_F$, the applied electric field initially places the nematic director in a position from which its controlling torques $M_\sigma^{\perp}$ and $M_\sigma^{\parallel}$ initiate EC domain rolls. These correlations of U_{th} and U_F, by using suitable LCC geometry or strong magnetic field orientation, may be expressed as an interplay between the periodic pattern formation and homogeneous modes reflected in a phenomenon such as dendritic growth [14–16]. In our case, with side-view geometry, smectic C order fluctuation and slightly positive ε_a, we observed such a phenomenon, provoked by the competition between a convection mode and a homogeneous mode, and leading to the induction of a subcritical hysteretic transition from the no-convection (quiescent) to the convection state. The critical frequency f_0 (different from the cutoff frequency f_c between conduction and dielectric regime in EC in conventional nematics), below which bifurcation between EC and Fréedericksz transition was indicated is also temperature-dependent [22]. Thus for each temperature in the N range of 8-OBA one can obtain different frequencies where U_{th} for EC could be larger or smaller than U_F. At U_{th}, in the EC dendrite picture onset, we expect the appearance of small dendrite nucleii. The outline of such dendrites increase for increasing $U>U_{th}$, with **E**$\perp$**n**.

In order to verify the subcritical EC behaviour we go to $U>U_F$ then apply different rates of voltage ramping (using a function generator), both up and down, as will be discussed later. A far larger effect however is the difference between the voltage at which convection appears when U is increasing and the voltage at which convection disappears when U is decreasing. Furthermore, in our exploration of the character of the bifurcation between convection and homogeneous Fréedericksz transition in the ramping-up, we observed by photodiode detection a very abrupt increase of the intensity of the transmitted (polarized) light, thus indicating the onset of planar director distortion at the crossed polarizers. These observation alone strongly indicate that for our conditions (ε_a small positive, smectic C order fluctuation and interplay of convection and homogeneous states), bifurcation from the quiescent state to the EC state is subcritical—discontinuous, hysteretic. We have repeated this exploration with a conventional nematic (PAA) as already mentioned, with different rates of ramping the voltage both up and down. However we have realized only surface-effected orientation (without the strong magnetic field used in [14–16]) and have not seen the onset of dendrite-like EC; we have thus not accomplished the transition to convection from the Fréedericksz distorted state. In this case convective rolls grow everywhere simultaneously, their intensity and corresponding contrast following the **n** distortions, growing continuously from zero, which is typical for a supercritical (forward) bifurcation.

Here we now discuss the method for identification of the parabolic character of the observed dendrite-like

textures. As mentioned above, the boundary between the quiescent state and the EC state has a finite width and is therefore much less sharp than the parabolic crystalline dendrites. Nevertheless, within the width of this diffuse boundary, there is a darkest point (see Figure 1) where the intensity has a minimum, as in the dendrites observed in [14–16]. The coordinates of the points corresponding to that intensity minimum define the outline of the dendrite. Thus we obtain a curve $z=z(x)$, which may be fitted to a second order polynomial $z=Ax^2+Bx+C$, indicating a parabola with tip point $x_o=B/2A$ and $z_o=(4AC-B^2)/4A$. The tip radius of curvature is now $\rho=1/|2A|$. The sign of A determines the direction of the parabolic tip in the ZX plane. For the dendrite in figure 1 we found $A=-0.097\pm 8$. The negative sign of A indicates that the parabola tip is in the positive Z direction. For comparison, the value of A obtained in [14–16] is -0.18, indicating a lower radius of curvature of the tip.

Before describing the measurement of geometrical and dynamical parameters typical for parabolic-type EC dendrites, we describe the electroconvectional characteristics of the dendrite onset; we take into account the peculiarity of EC in nematics with the short range smectic order of 8-OBA observed a in top-view LCC [22], as well as EC in a side-view LCC in the case of a conventional nematic (PAA). In order to take into account the contribution of an eventual isotropic instability caused by local charge injection, we perform the experiment by both non-blocked electrodes (silver wires) and blocked electrodes (lacquer isolator, tissue and polyimide coatings). We also restrict our analysis to dendrites appearing above T^* where $\sigma_a>0$. Thus we have a side-view LCC for 8-OBA at $T>T^*$, $\sigma_a>0$, and slightly positive ε_a. The case of EC below T^* where $\sigma_a<0$ will only be marked as an instability. This case will be subject of a future publication.

3.2. *Electroconvective characteristic of EC dendrite onset at unblocked lateral electrodes*

We are interested in the conduction regime the electroconvection; i.e. the critical onset voltage for EC dendrite formation as a function of frequency at different temperatures. A restriction to conducting EC is also made to avoid the dielectric regime (above cutoff frequency f_c) where a surface instability manifest as small scale vortices near both electrodes (side-view LCC) could be provoked [23, 29].

In figure 4 the dependence $U_{th}(f)$ for 8-OBA is shown for $d=300\,\mu m$, $h=50\,\mu m$. For the higher temperature range $T^*<T<T_{NI}$ (T^* is 130°C in this case), the $U_{th}(f)$ trend is: vanishing frequency dependence at low frequencies followed by a sharp increase in the 'conduction' regime and then a 'knee' at higher frequencies. The cutoff frequency, which is not clear in these nematics, increases with temperature. Below T^*, however, no such behaviour can be detected and U_{th} increases almost linearly with frequency. This trend below T^* demonstrate that the EC instability in this region has an underlying smectic-like behaviour.

The temperature dependence of the onset of EC dendrite texture is indicated in figure 5 for 8-OBA, $d=300\,\mu m$, $h=50\,\mu m$, $f=600\,Hz<f_c$, $T_{NI}=146°C$, $T_{NSmC}=108°C$. As can be seen, in the region of T^* (the plateau in $U_{th}(T)$ plot) the EC onset is achieved at

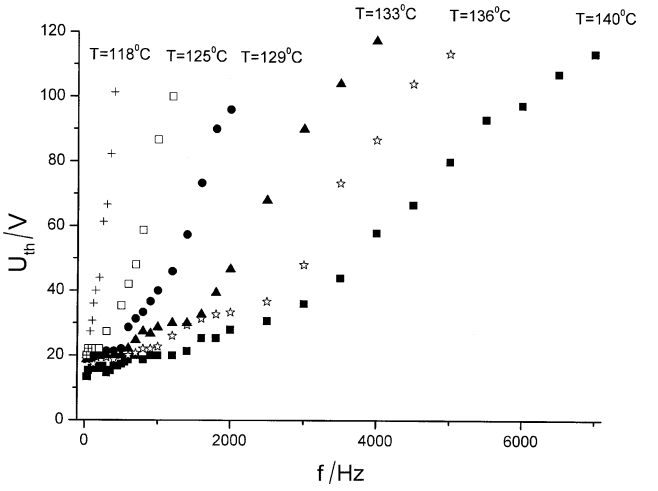

Figure 4. The $U_{th}(f)$ dependence at non-blocking electrodes at various temperatures above and below $T^*=130°C$. The LCC is side-view; the interelectrode distance $d=300\,\mu m$, film thickness $h=50\,\mu m$ (the silver wire thickness).

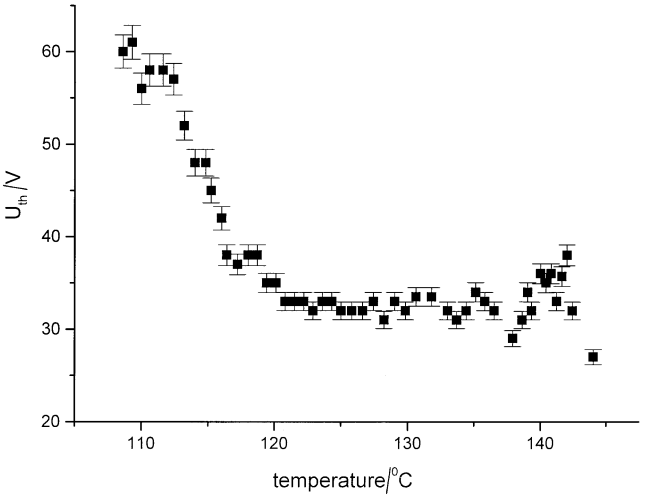

Figure 5. The $U_{th}(T)$ dependence at non-blocking silver electrodes; $d=300\,\mu m$, $h=50\,\mu m$, $f=600\,Hz$.

$U_{th} = const$. This effect reflects the interval where electric charge starts to spread out, with priority in quasi-layer planes. As already mentioned, we restrict our study to $T > T^*$, where smectic order fluctuations exist, but which are insufficient to change the sign of σ_a, which remains positive [31].

3.3. *EC dendrite growth and characteristics in blocked lateral electrodes*

The fundamental process underlying the described effect is based on a combination of charge transport and convection effects [25, 29]. We expect the blocking effect to change dramatically the charge distribution (potential gradient) between the electrodes. This effect is important mainly for d.c. excitation, where the charge injected by the negative electrode accumulates near to the positive electrode, thus creating an electric field gradient in the Z direction. However, we find that blocked electrodes are also important in the case of an a.c. applied field, where some injection could exist. To check such an injection we measured the $U_{th}(f)$ using various blocking layers. In figure 6 presents the dependences $U_{th}(f)$ for blocking by a polyurethane lacquer coating, for T above and below T^*; $d = 150\,\mu m$, $h = 60\,\mu m$. The thickness of the lacquer isolating layer is $5\,\mu m$, its dielectric constant $\varepsilon_L = 4.8$. We recall that the dielectric constant of *n*-OBA, on average, is ≈ 3.2 [21, 39, 40]. A surprising result can be seen for this dependence for the range $T > T^*$: $U_{th}(f)$ deviates from the normal trend (see figure 4) and a very high U_{th} value is obtained when $f \to 0$. Thus at low frequency we obtain electroconvection similar to that close to cutoff frequencies for EC in conventional (e.g. PAA) nematics, i.e. no electric charge distribution follows the application of an a.c. field, leading to **n** distortion oscillating as in the dielectric regime. Further increase of the frequency restores the system to a normal EC state, and one observes both conducting (500–700 Hz) and dielectric (above 700 Hz) regimes. One notes that the increasing $U_{th}(f)$ (which above 700 Hz could represent the onset of a dielectric regime) is in a frequency range rather lower than that of non-blocked electrodes. Thus we assume that the blocking to a great extent decreases the electric charge at low frequencies, leading to **n** oscillation and a 'frozen' charge, as in the dielectric regime but for very low frequencies. The observed minimum of the $U_{th}(f)$ ($f > 200$ Hz) trend can be explained by the insertion of addition electric charge. In this range the LC bulk carriers are unable entirely to screen the injected charges and the conduction state is realized (the molecular distortion is static and charges follow the electric field frequency). With further increase of f we almost repeat the trend typical for

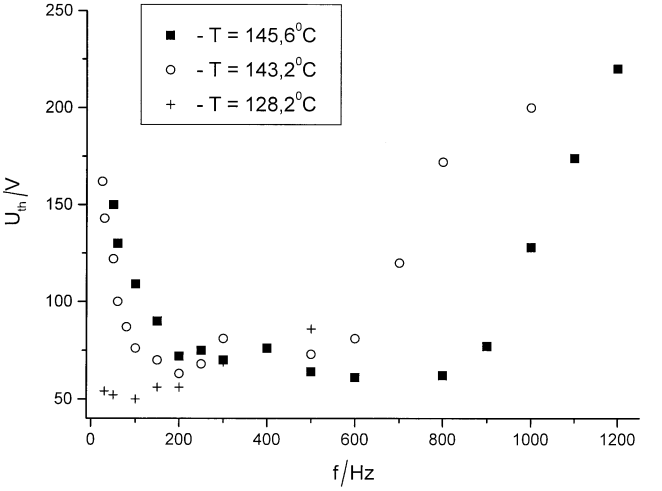

Figure 6. The $U_{th}(f)$ dependence at blocked electrodes (lacquer) for various T above and below T^*; $T^* = 130°C$, $d = 150\,\mu m$, $h = 60\,\mu m$.

unblocked electrodes but the full process (conductivity/dielectric state transition) manifests itself very quickly in respect to the frequency increase. As seen for temperatures below T^*, the typical minimum in $U_{th}(f)$ is not observed. On the contrary, at the same frequency (≈ 300 Hz) a maximum is seen. We assume that this is a result of the change of sign of σ_a from $\sigma_a > 0$ above T^* to $\sigma_a < 0$ below T^*. Thus below T^* screening of the charge injection by the bulk electric carriers is less effective.

An explanation (on a macroscopical level) of the U_{th} divergence as $f \to 0$ could be as follows: the potential drop across the LC (a remnant field between the isolating layers, because at finite frequencies, the electrical carriers in the nematic are unable to screen entirely the charges on the electrodes) decreases by an amount given by the capacity ratio of the layers, i.e. threshold voltage increase. The isolating layers introduced in the LCC system induces a capacitor–isolator between the ITO layer and the nematic, which we assume to be conducting (weak electrolyte, see [39]), and the voltage drop across the LC vanishes if the frequency goes to zero, thus U_{th} diverges.

An interesting analogy effect of the charge decrease due to electrode blockage is that if one takes a very pure substance, implying a very small bulk charge density, the dielectric regime (at $f > f_c$) characterized by sharply increasing U_{th}, may be achieved at frequencies tending to zero (see also [29]).

With for the polyimide coating we do not observe the typical $U_{th}(f)$ minimum as seen for a lacquer coating at temperatures below T^*; the voltage threshold frequency dependence is similar to that of unblocked electrodes.

The difference between lacquer and polyimide coatings is that the former is hydrophilic and the latter hydrophobic, implying that hydrogen bonding between liquid crystal molecules and the solid surface takes place, or not, in the respective cases. Presumably, due to the biphilic character of the open dimer and 'free' monomers, the screening effect in the case of the hydrophilic (lacquer) coating is more pronounced.

3.4. *Quantitative analysis of EC dendrite growth*

We now discuss the dynamics of EC dendrite growth in terms of the development with time of two quantities: the growth velocity $\mathbf{v}$ and the radius of curvature ρ of the parabolic tip. As a dimensionless controlling parameter, by analogy with the dimensionless supercooling at the thermal dendrites [14–16, 37] we define $\Delta=(U^2-U_{th}^2)/(U_c^2-U_{th}^2)$. We then vary Δ by varying U. Above U_{th}, dendrites appear via the front propagation mechanism. This growth mechanism demonstrates that the phenomenon is subcritical, with a large hysteresis. This is seen clearly in figure 7, as the applied voltage is ramped up and down, with U exceeding U_{th}, as described in § 3.1.

In the absence of surface tension between the dendrite and the host into which it grows, the boundary value problem for the diffusion equation may be solved exactly [14–16, 37]; and see the Ivantsov solution [36]. To obtain a parabolic two-dimensional solution, consider a uniformly propagating interface of shape $z(x,t)=z(x)+\mathbf{v}t$, where $z(x)=-x^2/2\rho$, corresponding to a parabola whose tip, of radius ρ, moves with velocity $\mathbf{v}$. In the absence of surface tension, a solution of the diffusion equation is obtained for the thermal crystal dendrite interface growth velocity, which is limited by the diffusion of latent heat L of melting away from interface [37]. Such an analogy was used in [14–16] and for EC liquid crystal dendrites.

A solution of the diffusion equation is thus obtained by choosing ρ or $\mathbf{v}$ to match the supercooling. The result is $\Delta=\pi P^{1/2}\exp(P)$, where $P\equiv\rho v/2D$ is the Peclet number and D is the diffusion constant [37]. However in this limit $\mathbf{v}$ and ρ are not independent; only the Peclet number can be determined from Δ. In [1], inclusion of the flow in consideration of dendrites led to complication of the study of the parabolic tip dendrite growth; the fundamental problem, in the absence of surface tension, is the existence of sufficient anisotropy, as the liquid crystals used in this study. Dendrites are stable only when sufficient anisotropy of the system is allowed for in the diffusion equation.

In figure 8 we plot $\rho\mathbf{v}$ against Δ for a large number of dendrites for the case of unblocked silver electrodes ($d=450\,\mu m$, $h=50\,\mu m$) and a d.c. field at $T=138^\circ C>T^*$. The velocities of dendrite growth ($\mathbf{v}_{resp}$) and decay (relaxation) ($\mathbf{v}_{rel}$) for the same experimental conditions are indicated in figures 9 (*a*) and 9 (*b*), respectively. It can be seen that $\mathbf{v}$ increases nonlinearly with U, while after removal the electric field, the relaxation velocity is constant, as expected.

Figures 10 (*a*) and 10 (*b*) show the $\Delta(\rho\mathbf{v})$ dependence for unblocked electrodes, with an a.c. lateral electric field applied by 50 μm silver electrodes ($d=450\,\mu m$, $T=138^\circ C>T^*$), at $f=25\,Hz$ and $f=250\,Hz$, respectively. At lower frequencies Δ is double that at the higher frequency. On comparing the $\Delta(\rho\mathbf{v})$ dependences for the same parameters (silver wire electrodes,

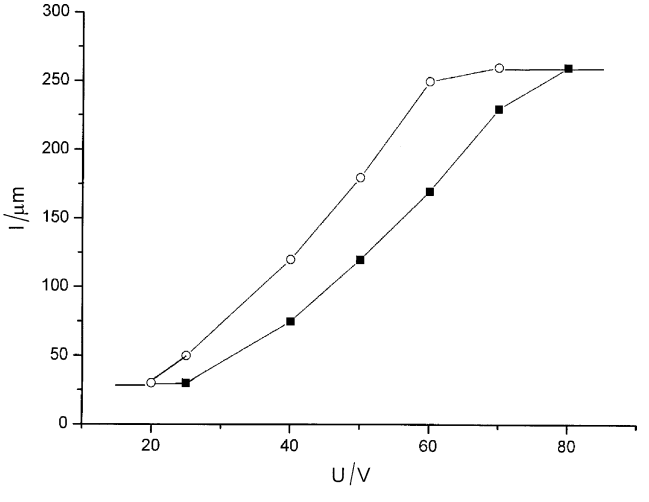

Figure 7. The subcritical (hysteretic) behaviour of the onset of EC dendrites, ○ U increaseing, ■ U decreasing: unblocked (silver) electrodes, $d=450\,\mu m$, $h=50\,\mu m$, $T=138^\circ C>T^*$.

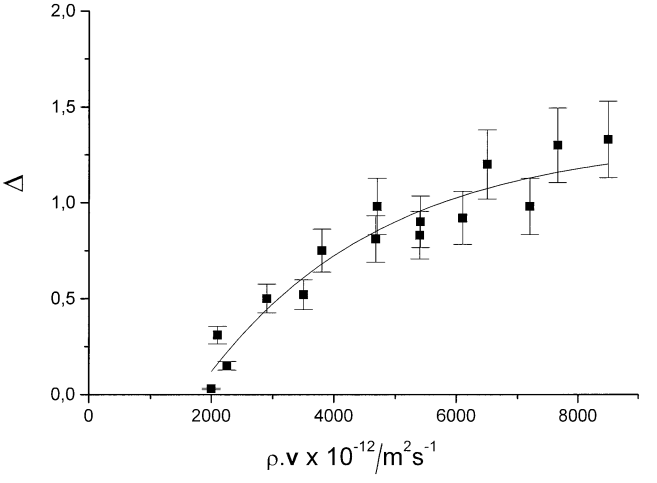

Figure 8. The $\Delta(\rho\mathbf{v})$ dependence at unblocked electrodes, $d=450\,\mu m$, $h=50\,\mu m$ in a d.c. electric field with $T=138^\circ C>T^*$.

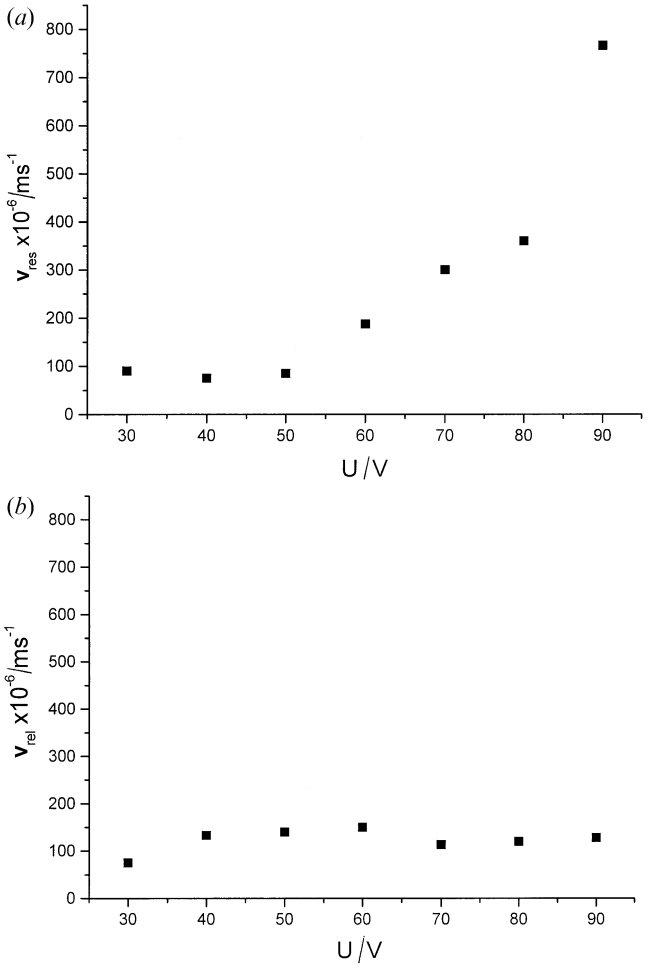

Figure 9. The growth (*a*) and relaxation (*b*) velocities for $T=138^{\circ}\mathrm{C}>T^{*}$ at unblocked electrodes, $d=450\,\mu\mathrm{m}$, $h=50\,\mu\mathrm{m}$.

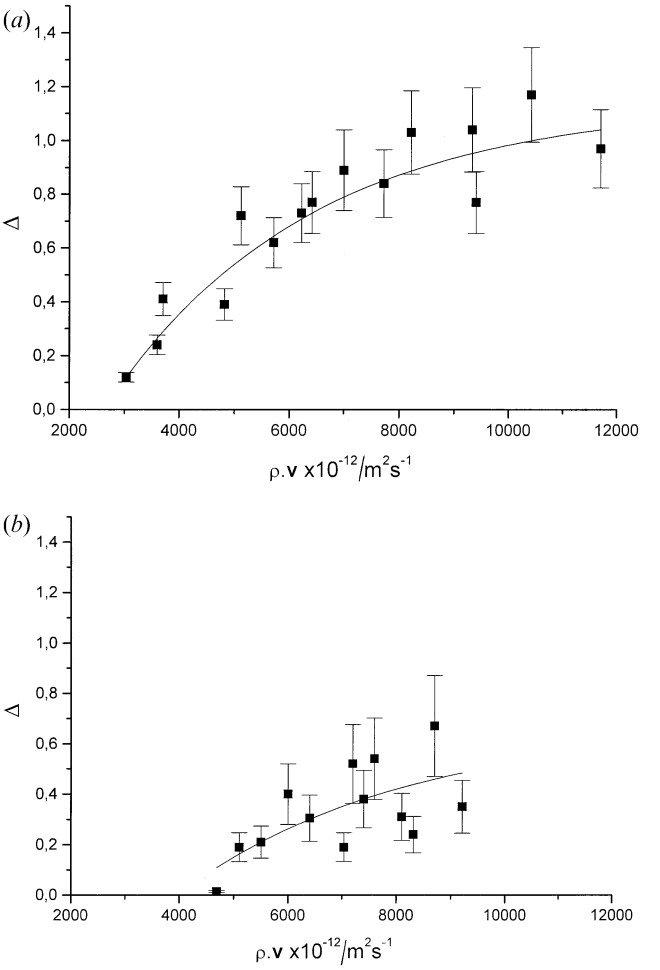

Figure 10. The $\Delta(\rho v)$ dependence at $f=25\,\mathrm{Hz}$ (*a*) and $f=250\,\mathrm{Hz}$ (*b*) in unblocked electrodes, $d=450\,\mu\mathrm{m}$, $h=50\,\mu\mathrm{m}$, $T=138^{\circ}\mathrm{C}>T^{*}$.

$d=450\,\mu\mathrm{m}$, $T=138^{\circ}\mathrm{C}>T^{*}$) it can be seen that Δ for d.c. is larger than for a.c. This implies that because of injection (the bulk carriers cannot entirely screen charge injection from unblocked electrodes) ion transport in the d.c. case is somewhat impaired. Such an effect is expected since injection by the negative electrode leads to charges pile-up on the positive electrode, thus providing an electric field gradient in the Z direction (opposite to the direction of dendrite growth).

In figure 11 we show $\Delta(\rho\mathbf{v})$ dependences for polyimide coated blocked electrodes, $h=60\,\mu\mathrm{m}$, for $T=138^{\circ}\mathrm{C}>T^{*}$, $d=250\,\mu\mathrm{m}$, at 1 kHz. We found that a Δ value of 0.4 ($\rho\mathbf{v}=8\times10^{-12}\,\mathrm{m^{2}\,s^{-1}}$) for the d.c. case, decreases to 0.25 ($\rho\mathbf{v}=8\times10^{-12}\,\mathrm{m^{2}\,s^{-1}}$) for an a.c. of 1 kHz. This means that the $\rho\mathbf{v}$ value is frequency-independent and that with on a.c. field, although with blocked electrodes, we have an opposing charge transport, which provides an electric field gradient in the Z direction. For the lacquer case in an a.c. field at

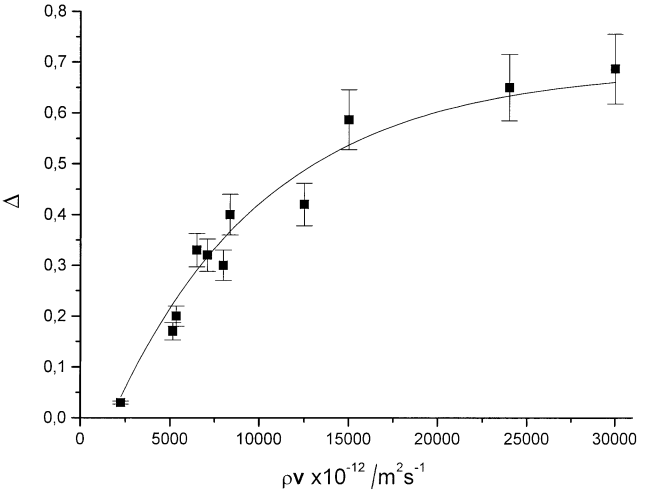

Figure 11. The $\Delta(\rho\mathbf{v})$ dependence for polyimide blocked electrodes, $d=250\,\mu\mathrm{m}$, $h=60\,\mu\mathrm{m}$ with on a.c. electric field for $f=1\,\mathrm{kHz}$ and $T=138^{\circ}\mathrm{C}>T^{*}$.

100 Hz the effect is the same. However, on comparing with unblocked electrodes, figures 8–10, it can be seen that Δ (for the same $\rho\mathbf{v}=8\times10^{-12}\,\mathrm{m^2\,s^{-1}}$) both for d.c. and a.c. is almost twice that for unblocked electrodes. One conclusion could be that in the case of blocked electrodes the opposing charge transport and electric field gradient in the Z direction are smaller.

The relative uncertainty in determining the velocity at higher voltage is about 15%. Thus, the tip velocity $\mathbf{v}$ is not uniquely selected by U, in contrast to the results of measurements on thermal dendrites described in [35]. As shown in figures 8–11 for unblocked and blocked electrodes, the product of the average ρ and $\mathbf{v}$ follows the typical curve for the two-dimensional diffusion equation solution for anisotropic crystalline dendrite growth [14–16, 37]. The solid line is a fit to the relationship between Δ and Peclet number P yielded by the solution of $\Delta=\pi P^{1/2}\exp(P)$.

Using our approximate value of $\rho\mathbf{v}$, from the different trends (figures 8–11) for the unblocked and blocked electrodes, we can estimate the relevant diffusion constants to be a set of values $\approx10^{-7}\,\mathrm{cm^2\,s^{-1}}$. In all cases this is within a half of the orientational diffusion constant (the ratio of the splay elastic constant to the rotational viscosity [25]) for the nematic director, implying that the diffusion field controlling this dendrite growth has the orientation of $\mathbf{n}$. Here we can give only a qualitative evaluation, that the diffusion constant D varies in the different cases of blocked and unblocked electrodes, with, respectively, d.c. and a.c. excitation. The decrease of the diffusion constant at unblocked electrodes could be a result of the opposing charge transport.

The outline of the EC dendrites (see figure 1) can be thought of as the transition region between the area in which the liquid crystal is stationary and the area in which convective flow occurs. This transition region, as measured by the width of the interface between the convective and the quiescent states is fairly wide, a consequence of the smooth variation of the orientation of the nematic director across this interface, which is a domain wall for the $\mathbf{n}$ topology. Such a transition region (front) is characteristic for non-equilibrium pattern formation and is analogous to a first order phase transition, with only one significant difference: it takes place in a thermodynamically monophase system [15, 17].

4. Suggested mechanism of the dendrite growth

Theory [9, 25, 29] does not explain either a transition to a time-dependent state expressed as localized domains of travelling rolls [13, 32] or EC dendrite front propagation. The most common in the electroconvective stationary and time-dependent states pattern, thus including EC dendrites in liquid crystals, are their fundamental property: intrinsic anisotropy of the electroconductivity providing a separation and pilling up of charge in the direction perpendicular to the applied electric field and by turns in convective flow.

While there are classical [25, 29] and contemporary [9, 34] theories for EC in standard geometry (top-view), which seem to be applicable to EC in nematics, no such theory exists for the side-view/lateral electrodes case with nematics characterized by strong smectic order fluctuations. The main difference in these systems is that the interelectrode distance in top-view cells in respect to the LC film dimension (XY) is rather small, and the EC flow (as indicated by small particles) is visualized in the XZ plane, which is perpendicular to the planes of the glass plates.

The LCC used by us for dendrite observation gives the possibility of observing the front propagation and detecting the flow by small particles in the XZ plane, now parallel to the planes of the glass plates. In this case we observed travelling rolls bent in a parabolic shape. The known Carr–Helfrich mechanism could therefore be adapted to the travelling rolls in, where the subcritical bifurcation between EC and Fréedericksz states is pronounced.

There is one notable difference between crystalline or thermal LC dendrites [1–8, 35, 37] and the EC dendrites observed by us and Gleeson *et al.* [14–16] for various liquid crystals, geometry and external LC orientations. In thermal dendrite growth the moving interface between two states (stable and metastable) is accompanied by attachment of the molecules of the supercooled liquid to the growing solid (or supercooled N to the growing smectic for liquid crystals). Thus the driving force in the dynamics of thermal dendrites (determining the rate of growth) is the diffusion of latent heat of melting away from the interface. For the travelling parabolic rolls manifesting subcritical bifurcations between already distorted (in a strong magnetic field) Fréedericksz and EC states [14–16] and those observed by us, the driving force is provided by the coupling between the electric charge (distributed, due to the electroconductivity anisotropy) and the applied electric field. Strong hysteresis is also typical for EC dendrites. It may be noted that at the supercritical (forward) bifurcation commonly observed in conventional nematics (in the absence of a strong magnetic field), primary (NR) and secondary EC instabilities only are observed.

Using 8-OBA, characterized with strong smectic C order fluctuation and very small ε_a in top-view geometry, we observed at T^* a transition between roll (tilted in respect to $\mathbf{n}_o\equiv X$) and cell-like domains (see figure 3); but no propagating, parabolic shaped

dendrite texture was seen. We presume that this is due to the roles of the onset Leslie coefficients α_3 and α_2, fundamental in EC, when the LCC geometry and LC material constants are changed. As indicated above, these coefficients are included in the two torques controlling the liquid flow balance: (i) $M_\sigma^{\perp} = -\alpha_2|\partial v_z/\partial x|$ [29], destabilizing in our side-view geometry after the Fréedericksz distortion, and (ii) the stabilizing torque $M_\sigma^{\parallel} = \alpha_3|\partial v_x/\partial z|$. Assuming bend deformation in the XZ plane, and the gradients $\partial v_x/\partial z$ and $\partial v_z/\partial x$ to be comparable, the role of the stabilizing torque $M_\sigma^{\parallel}$ in this two-dimensional consideration could lead to an enhancement of the threshold value of the driving voltage (since $\alpha_3 < \alpha_2$), which we actually detect. Such an effect leads to enhancement of the subcriticality, since the EC onset occurs after the stronger initial Fréedericksz distortion.

Thus a possible explanation of the effect could be the influence of the boundary conditions on the EC in our experiment. In the side-view case used here, the boundary effect is rather more complex (than in the top-view case) and appears as a result of the two boundary interfaces: (i) the interface between the LC and solid electrodes, and (ii) the interface between the two plates and the oriented liquid crystal. This surface field certainly modifies the **n** distortion, and the α_3, α_2 signs and values, and presumably enhances the stabilizing torque $M_\sigma^{\parallel}$ as mentioned. This torque enhancement could cause the increase in U_{th}, following the E_{F} increase, and as a result provides the subcriticality described above. Up to now however we cannot take account of this in our consideration. The difference of the electrochemistry at the differing electrodes is also important.

Essential information for the description of the velocity field is obtained from direct observation of the paths of the small (3–5 μm) particles immersed in the LC, a method widely used for EC study. By this method we clearly find a trajectory indicating an open motion, in which the particles move up and down between the rolls and simultaneously translate in a sense opposite to that of the media of the rolls, maintaining a slightly lower rate. Such an open stream usually extends away from the dendrite outline, where it develops a large scale flow velocity, which measured at the EC threshold condition $U_{\mathrm{th}}(f)$ dependence, is about one order smaller than that of the dendrite interface growth rate.

Although the existing one-dimensional theory [25, 29] is unable to account for the spatio–temporal dependences appearing here at pattern formation, it does show that the molecular orientation relaxation time becomes comparable to the ionic relaxation time at frequencies approaching the cut-off frequency. The result is a loss of efficiency of the focusing mechanism by the molecular alignment curvature, which leads to a significant increase of the threshold voltage. The time periods responsible for this effect are charge relaxation time τ, the **n** curvature relaxation time τ_{c}, the transit time of ions τ_{i} and time τ_{f} of convective flow over the rolls. The times are defined as [29]: $\tau_{\mathrm{i}} = d/\mu\mathbf{E}$, where μ is the ionic mobility; $\tau = \varepsilon_{\parallel}/4\pi\sigma_{\parallel}$; $\tau_{\mathrm{c}}^{-1} = \gamma^{-1}[(-\varepsilon_{\mathrm{a}}\varepsilon_{\perp}/4\pi\varepsilon_{\parallel})\mathbf{E}^2 + K_{33}q^2]$, where K_{33} is the bend elastic constant, q the wave vector and γ the bend viscosity [25]. The values of τ_{f} deduced from the experiment are of order of 4 s. The other numerical values are: τ_{i} on average ≈ 0.8 s, $\tau \approx 4 \times 10^{-3}$ s, $\tau_{\mathrm{c}} \approx 30 \times 10^{-3}$ s. The value $\mu \approx 3 \times 10^{-5}\,\mathrm{cm^2\,s^{-1}\,V^{-1}}$ was taken from [41] and the other material constants from [25, 29, 31]. The values of τ and τ_{c} are average and are estimated for a frequency interval close to, but below the cut-off frequency (figure 4), where U_{th} significantly increases. Therefore, since τ_{c} and τ are comparable in this interval, the curvature there is less efficient in maintaining the charge modulation stable in space against any possible lateral drift. In fact, for a slight lateral shift (along the wave vector direction Z) of the charge distribution, and within each half-period of the electric field (in the a.c. case), the curvature $\partial\varphi/\partial x$, will immediately adapt to the new distribution. Here we assume that for normal focusing (molecular alignment curvature ensuring EC pictures with high contrast) the initial alignment of the charge distribution due to electrocondictivity anisotropy ($\sigma_{\mathrm{a}} > 0$ above T^*) is in the X direction. Thus lateral drift of the charge distribution along the dendrite growth direction Z may occur in the presence of a conductivity gradient $\mathrm{d}\sigma/\mathrm{d}z$, which contributes to a current density $\delta J = \mu\delta Q E_z$ along Z. Then the charge density distribution takes a form such as $Q = Q_0 \cos q(z - \mathbf{v}t)$ ($q = 2\pi/d$, the wave number) from which one may define a frequency $W = q\mathbf{v}/2\pi = \omega/2\pi \neq f$. Onto the molecular orientation φ variation is then superimposed a slow component $\varphi_{\mathrm{o}} \cos(\omega t - qz)$. The angle φ now fluctuates around X with typical frequency $W = 0.2$ Hz (for $\mathbf{v} = 10$ μm/s, $q = 10^3\,\mathrm{cm^{-1}}$), which may be compared with the excitation frequencies f (100–1000 Hz in the experiment). As previously indicated [29, 30] such a fluctuation in respect to the $\mathbf{n}_{\mathrm{o}}$ easy direction provides rolls tending to be parallel to this direction. Such rolls in standard a LCC could also be tilted in respect to $\mathbf{n}_{\mathrm{o}}$ as indicated figure 3 (*a*). Thus the overall pattern (EC dendrite outline) moves as a progressive wave in a direction perpendicular to the molecular orientation $\mathbf{n}_{\mathrm{o}}$, along with a charge-density wave as, for example in convection in binary mixtures [18].

The suggested mechanism could account for the opposing ion transport which is more pronounced in the case of unblocked electrodes. One would expect that

in the case of ideal blocking of the electrodes and depression of the lateral drift, the propagating front would move parallel to the electrodes. We assume that the parabolic outline of the EC dendrites seen in figure 1 indicates the competition between ion transport in the $+Z$ and $-Z$ directions. As already mentioned, the black and white stripes indicate EC rolls which, contrary to the known Williams domains (NR), follow the direction of the initial molecular orientation. These rolls in many aspects resemble the EC domains pattern in top-view (vertical XZ section) with longitudinal domain lines [29, 30] but deformed in a parabolic form as a result of the electric field gradient in the Z direction.

Using polyimide (hydrophobic) and lacquer (hydrophilic) coatings, and thus the amphiphilic properties of dimerized molecules of *n*-OBA, one expects to be able to control charge injection; the double electric layer as well as the adsorption of the lateral electrodes. This property of *n*-OBA is useful in furthering the understanding of the mechanism of EC dendrite growth, which will be a future task. In considering the thermal dendrites observed in 8-OBA [35] together with the EC dendrites in the same substance, we found that they possess different morphological and dynamical characteristics, but both obey growth mechanisms that indicate a weak first order phase transition, with front propagation and a distinct hysteresis.

While the mechanism of the thermal dendrites excludes fluid flow, in EC dendrites the flow become a basic characteristic. The subcritical (hysteretic) property of EC dendrites observed by us (which could be a result of both smectic order fluctuation, small $\varepsilon_a > 0$ in the N state of 8-OBA and opposite charge transport in a lateral electric field), also relates this phenomenon to a first order phase transition, but in a thermodynamically monophase system.

Some apparently similarities in the EC dendrites observed here [14–16] and in crystalline dendrites are: (i) the growth morphology by which one state is replaced by another (quiescent–convective); (ii) front moving at constant speed without changing the parabolic shape (in the frame of reference moving at the growth velocity); (iii) consistency with the constitutive relationship for the two-dimensional Ivantsov solution. Some important differences however are: (i) the growth is not controlled by diffusion of a conserved quantity; (ii) there are no sidebranch tips.

5. Conclusion

We have observed for the first time electroconvective dendrites (parabolic type) in nematics with short range smectic order such as 8-OBA. The driving of the dendrites is carried out by lateral d.c. and a.c. electric field parameters above the temperature T^* (dividing the N phase of *n*-OBA into a high temperature N_1 classic-like phase, and a low temperature N_2 smectic-like phase) in the nematic temperature range. The dynamics of the dendrite growth was studied and an analysis by the Ivantsov two-dimensional solution for the diffusion equation is presented; the large anisotropy of the liquid crystal substance allows such an analysis. Using various combinations of blocked and unblocked electrodes, and liquid crystal geometries, we studied the frequency dependence of the threshold for EC dendrite appearance as well as the dependence $\Delta(\rho v)$ (between the dimensionless electric field parameter and the product of the dendrite parabolic radius and the velocity of dendrite growth) and found that the blocked and unblocked electrodes, for a temperature above T^*, significantly modify these basic dependences. We relate this effect to the possible opposing ion propagation (electric field gradient in the direction opposite to that of the charge injection). The role of the different degrees of charge injection is also discussed. The observed subcritical and hysteretic character of EC dendrite formation is analysed by these effects. A possible mechanism is suggested, similar to that of classical EHDI in nematics, but accounting for the drift of the charge distribution in the direction of EC dendrite growth.

Finally a comparison with thermal LC dendrites is presented. The common feature of thermal and EC dendrites is found to be the front propagation and distinct hysteresis of their onset and disappearance, relating these phenomena to a first order phase transition. The parabolic form of the EC dendrites (optically seen as black and white stripes of minimum and maximum intensity) is analysed assuming that the EC roll (longitudinal type) is curved due to lateral charge drift in the $\pm Z$ direction. We believe that a future theory of the transition to a time-dependent and space-localized EC state may be able to explain a phenomenon such as liquid crystal dendrites controlled by the electric field parameters.

This study was supported by Grant No. 1307 from the Ministry of Education and Science of Bulgaria.

References

[1] JEONG, J. H., GOLDENFELD, N., and DANTZIG, J. A., 2001, *Phys. Rev. E*, **64,** 041602.
[2] HURLE, D. (editor), 1993, *Handbook of Crystal Growth*, Vol. 1B (Amsterdam: North-Holand).
[3] TOTH-KATONA, T., BORZSONYI, T., SZABON, J., and BUKA, A., 1996, *Phys.Rev. E*, **54,** 1574.
[4] BEN-JACOB, E., and GARIC, P., 1990, *Nature*, **343,** 523.
[5] BUKA, A., and EBER, N., 1993, *Europhys. Lett.*, **21,** 477.
[6] BUKA, A., KATONA, T., and KRAMER, L., 1995, *Phys. Rev. E*, **51,** 571.

[7] BUKA, A., PALFFY-MUHORAY, P., and RACZ, Z., 1987, *Phys. Rev. A*, **36,** 3984.
[8] ARORA, S., BUKA, A., PALFFY-MUHORAY, P., RACZ, Z., and VORA, R., 1988, *Europhys. Lett.*, **7,** 43.
[9] KRAMER, L., and PESCH, W., 1996. In *Pattern Formation in Liquid Crystals*, edited by A. Buka and L. Kramer (New York: Springer).
[10] SCHATZ, M., VAN HOOK, S. J., MCCORMICK, W., SWIFT, J., and SWINNEY, H., 1995, *Phys.Rev. Lett.*, **75,** 1938.
[11] EBER, N., NEMETH, S., ROSSBERG, A. G., KRAMER, I., and BUKA, A., 2002, *Phys. Rev. E*, **66,** 036213.
[12] SHI, J., WANG, C., SURENDRANATH, V., KANG, K., and GLEESON, J. T., 2002, *Liq. Cryst.*, **29,** 877.
[13] JOETS, A., and RIBOTTA, R., 1986, *J. Phys. (Paris)*, **47**, 595; JOETS, A., and RIBOTTA, R., 1988, *Phys. Rev. Lett*., **60**, 2164.
[14] GLEESON, J. T., 1997, *Nature*, **385,** 511.
[15] GLEESON, J. T., 1996, *Phys. Rev. E*, **54,** 6424.
[16] CHEORGHIU, N., and GLEESON, J. T., 2002, *Phys. Rev. E*, **66,** 051710.
[17] CLADIS, P. E., VAN SAARLOOS, W., HUSE, D. A., PATEL, J. S., GOODBY, J. W., and FINN, P. L., 1989, *Phys. Rev. Lett.*, **62,** 1764.
[18] BRAND, H. R., LOMDAHL, P. S., and NEWEEL, A. C., 1986, *Physica (Amsterdam)*, **23D**, 345; BRETHERTON, C. S., and SPEIEGEL, E. A., 1983, *Phys. Lett*., **96**, 152.
[19] PETROV, M. P., and SIMOVA, P. D., 1985, *J. Phys. D*, **18,** 239.
[20] NEUBERT, M., and DE VRIES, A., 1985, *Mol. Cryst. liq. Cryst.*, **145,** 1.
[21] FRUNZA, S., FRUNZA, A., SPARAVIGNA, A., PETROV, M. P., and TORGOVA, S. I., 1996, *Mol. Mater.*, **6,** 215.
[22] SIMOVA, P., and PETROV, M., 1981, *J. Phys. D*, **14,** 1.
[23] HUH, J.-H., and KAI, S., 2003, *Phys Rev. E*, **68,** 042702.
[24] KAI, S., YAMAGUCHI, K., and HIRAKAWA, K., 1975, *Jpn. J. appl. Phys.*, **14,** 1653.
[25] DE GENNES, P. G., and PROST, J., 1993, *The Physics of Liquid Crystals* (Oxford: Clarendon Press).
[26] PLANT, E., DECKER, W., ROSSBERG, A. G., KRAMER, L., PESH, W., BELAIDI, A., and RIBOTTA, R., 1997, *Phys. Rev. Lett.*, **79,** 2367.
[27] RICHTER, H., BUKA, A., and REHBERG, I., 1995, *Phys Rev. E*, **51,** 5886.
[28] HUH, J.-H., HIDAKA, Y., and KAI, S., 1998, *Phys. Rev. E*, **58,** 7355.
[29] BLINOV, L. M., and CHIGRINOV, V. G., 1994, *Electro-optical Effects in Liquid Crystal Materials* (New York: Springer-Verlag).
[30] BARNIK, M. D., BLINOV, L. M., GREBENKIN, M. F., PIKIN, S. A., and CHIGRINOV, V. G., 1975, *Phys. Lett. A*, **51,** 175.
[31] CUVATOV, Z. X., CAPASTIN, A. P., and TROFIMOV, A. N., 1976, *Pisma JETP*, **19,** 89.
[32] BRAND, H. R., FRADIN, C., FINN, P. L., PESCH, W., and CLADIS, P. E., 1997, *Phys. Lett. A*, **235,** 508.
[33] BUKA, A., DRESSEL, B., OTOWSKI, W., CAMARA, K., TOTH-KATONA, T., KRAMER, L., LANDAU, J., PELZL, G., and PESCH, W., 2002, *Phys. Rev. E*, **66,** 051713.
[34] DRESSEL, B., and PESCH, W., 2003, *Phys. Rev. E*, **67,** 031707.
[35] MARCEROU, J. P., PETROV, M., NARADIKIAN, H., and NGUYEN, H. T., 2004, *Liq. Cryst.*, **31,** 311.
[36] IVANTSOV, G. P., 1947, *Dokl. Acad.Nauk.SSSR*, **58,** 567.
[37] KESSLER, D. A., KOPLIK, J., and LEVINE, H., 1988, *Adv. Phys.*, **37,** 255.
[38] VAN SAARLOOS, W., 1989, *Phys. Rev. A*, **39,** 6367.
[39] PETROV, M., BRASLAU, A., LEVELUT, A. M., and DURAND, G., 1992, *J. Phys. II Fr.*, **2,** 1159.
[40] PETROV, M., and DURAND, G., 1996, *J. Phys. II (Fr.)*, **6,** 1259.
[41] ATTEN, P., MALRAISON, B., and KANI, S., 1982, *J. Elecrostat.*, **12,** 477.